Skyrmion-based logic gates controlled by electric currents in synthetic antiferromagnet

Linlin Li(李林霖)[1], Jia Luo(罗佳)[1], Jing Xia(夏静)[2], Yan Zhou(周艳)[3], Xiaoxi Liu(刘小晰)[2], and Guoping Zhao(赵国平)[1,4,†]

[1] *College of Physics and Electronic Engineering, Sichuan Normal University, Chengdu* 610068, *China*
[2] *Department of Electrical and Computer Engineering, Shinshu University, Wakasato* 4-17-1, *Nagano* 380-8553, *Japan*
[3] *School of Science and Engineering, The Chinese University of Hong Kong, Shenzhen* 518172, *China*
[4] *Center for Magnetism and Spintronics, Sichuan Normal University, Chengdu* 610068, *China*

(Received 26 July 2022; revised manuscript received 28 September 2022; accepted manuscript online 18 October 2022)

Skyrmions in synthetic antiferromagnetic (SAF) systems have attracted much attention in recent years due to their superior stability, high-speed mobility, and completely compensated skyrmion Hall effect. They are promising building blocks for the next generation of magnetic storage and computing devices with ultra-low energy and ultra-high density. Here, we theoretically investigate the motion of a skyrmion in an SAF bilayer racetrack and find the velocity of a skyrmion can be controlled jointly by the edge effect and the driving force induced by the spin current. Furthermore, we propose a logic gate that can realize different logic functions of logic AND, OR, NOT, NAND, NOR, and XOR gates. Several effects including the spin–orbit torque, the skyrmion Hall effect, skyrmion–skyrmion repulsion, and skyrmion–edge interaction are considered in this design. Our work may provide a way to utilize the SAF skyrmion as a versatile information carrier for future energy-efficient logic gates.

Keywords: skyrmions, logic gates, synthetic antiferromagnets, micromagnetic simulation

PACS: 75.50.–y, 75.78.Cd, 85.70.Ay, 12.39.DC **DOI:** 10.1088/1674-1056/ac9b01

1. Introduction

Magnetic skyrmion is a particle-like spin configuration with quantized topological number, which was first proposed by Skyrme in 1962.[1] Afterward, the isolated skyrmion was theoretically predicted in various magnetic systems,[2,3] such as in liquid crystal,[4] non-centrosymmetric bulk magnets and thin films.[5–11] Recently, extensive experiments have observed skyrmions stabilized by the Dzyaloshinskii–Moriya interaction (DMI) at room temperature.[8,12–17] Due to their nanosize, high mobility and topological protection, skyrmions can be regarded as the prominent binary data carrier in advanced memories,[18–22] logic gates and computing devices.[23–25] In particular, the presence of a skyrmion represents the data bit "1", while the absence of a skyrmion denotes the data bit "0".[26–32]

Various ways have been proposed to realize the motion of skyrmions in a racetrack,[33–36] including the spin-polarized current, the temperature gradient, the magnetic anisotropy gradient, *etc*.[29,37,38] However, the ferromagnetic (FM) skyrmion will exhibit a lateral drift during the motion (*i.e.*, the skyrmion Hall effect) due to the presence of Magnus force,[39–41] which may cause the annihilation of skyrmions at the racetrack edge and thus destroy the information.[29] Therefore, interest has been devoted to SAF skyrmions that can effectively suppress the skyrmion Hall effect without affecting the topological protection.[31,42–45] Up to now, there are many logic devices that have been designed based on skyrmions and domain wall (DW) dynamics in nanotrack, such as the reversible conversion and the collision between the skyrmion and the domain wall,[23,24,26,46,47] skyrmion–skyrmion collision,[27,40,48–50] skyrmion Hall effect and skyrmion–edge repulsion.[40] Compared with the most investigated FM skyrmions and domain wall, the racetrack memory and logic devices based on SAF skyrmions exhibit five distinctive characteristics. Firstly, SAF skyrmions can move straight along the spin-polarized current without the skyrmion Hall effect.[42] Secondly, it can robustly protect the magnetic perturbation as the net magnetization of skyrmion is zero.[42] Thirdly, SAF skyrmion can move at higher velocity driven by spin currents than FM skyrmion and domain wall.[31] Fourthly, logic devices only use skyrmion's motion and interaction without the reversible conversion between skyrmions and DW, which can effectively decrease the complexity of logic implementation.[27,28] Fifthly, the SAF-skyrmion-based logic gates can simplify the driving mode of devices, reducing energy consumption, enhancing the motion speed of skyrmion and increasing the types of logic functions.[30]

In this work, we have analyzed the skyrmion motion velocity of SAF skyrmion in SAF racetracks and found the velocity can be influenced by the edge and driving force,[46,51] which agrees very well with the simulation results. Further,

†Corresponding author. E-mail: zhaogp@uestc.edu.cn

© 2023 Chinese Physical Society and IOP Publishing Ltd

we computationally propose a complete logic gate on SAF skyrmions including AND, OR, NOT, NOR, XOR, and NAND gates by utilizing the spin–orbit torque,[52–54] skyrmion Hall effect,[42,55,56] skyrmion–skyrmion repulsion, and skyrmion–edge interaction.[40,57] In the SAF bilayer, we show that bilayer-skyrmion can travel along the racetrack at a high speed driven by spin current, which is beneficial to simplify the operation of skyrmion-based devices.

2. Model and methods

Figure 1(a) illustrates the proposed structure, which is composed of two perpendicularly magnetized FM layers strongly coupled via the antiferromagnetic (AFM) interface interaction with a heavy metal layer beneath the bottom FM layer.[42] For the current-induced SAF skyrmion dynamics, we apply electric current in the $+x$ direction in the heavy metal (HM) layer to produce a vertical spin current to the magnetic layer and numerically solve the modified Landau–Lifshitz–Gilbert (LLG) equation including the damping-like spin–orbit-torque in the simulation. Here, the time-dependent magnetization dynamics is thus governed by[29,58]

$$\begin{aligned}\frac{\mathrm{d}\boldsymbol{m}_i}{\mathrm{d}t} &= -\gamma_0 \boldsymbol{m}_i \times \boldsymbol{h}_{\mathrm{eff}} + \alpha\left(\boldsymbol{m}_i \times \frac{\mathrm{d}\boldsymbol{m}_i}{\mathrm{d}t}\right) \\ &\quad + \gamma_0 u \boldsymbol{m}_i \times (\boldsymbol{m}_i \times \boldsymbol{p}),\end{aligned} \tag{1}$$

where $\boldsymbol{h}_{\mathrm{eff}} = -\partial H_{\mathrm{total}}/\mu_0 M_{\mathrm{s}} \partial m_i$ is the effective magnetic field induced by the free energy density of the system, μ_0 is the vacuum magnetic permittivity and M_{s} is the saturation magnetization. $\boldsymbol{m}_i$ represents the local magnetic moment orientation, γ_0 is the gyromagnetic ratio and α is the Gilbert damping coefficient, and $\boldsymbol{p} = -\hat{y}$ represents a spin polarization vector.

$$\gamma_0 u = \left|\frac{\hbar}{\mu_0 e}\right| \frac{j\theta_{\mathrm{SH}}}{2aM_{\mathrm{s}}}$$

is the damping-like spin–orbit-torque coefficient with $\hbar$ as the reduced Planck constant, e is the electron charge, j is the applied driving current density, $\theta_{\mathrm{SH}} = 0.1$ is the spin Hall angle, a is the film thickness of FM layer. For the total Hamiltonian H_{total}, we consider the Hamiltonian of each FM layer H_n and the interlayer AFM exchange coupling H_{inter} between the top and bottom FM layers,[42,59] which can be written as

$$H_{\mathrm{total}} = \sum_{n=\mathrm{T,B}} H_n + H_{\mathrm{inter}}. \tag{2}$$

The Hamiltonian for each FM layer can be written as follows:

$$\begin{aligned}H_n &= -A_{\mathrm{intra}} \sum_{\langle i,j\rangle} \left(\boldsymbol{m}_i^n \cdot \boldsymbol{m}_j^n\right) + K \sum_i \left[1 - \left(\boldsymbol{m}_i^{n,z}\right)^2\right] \\ &\quad + \sum_{\langle i,j\rangle} \boldsymbol{D} \cdot \left(\boldsymbol{m}_i^n \times \boldsymbol{m}_j^n\right) + H_{\mathrm{DDI}},\end{aligned} \tag{3}$$

where n is the FM layer index ($n = \mathrm{T}$, B represents the top layer and bottom layer, respectively), $\boldsymbol{m}_i^n$ denotes the local magnetic moment orientation normalized as $|\boldsymbol{m}_i^n| = 1$ at the site i, and the $\langle i, j\rangle$ runs over all the nearest-neighbor sites in each FM layer. The first term represents the intralayer FM exchange interaction with FM exchange stiffness $\boldsymbol{A}_{\mathrm{intra}}$. The second and third terms represent the perpendicular magnetic anisotropy with the anisotropy constant K and the DMI with the DMI vector $\boldsymbol{D}$, respectively, while H_{DDI} represents the dipole–dipole interaction. The Hamiltonian for the interlayer AFM exchange interactions can be written as follows:

$$H_{\mathrm{inter}} = -A_{\mathrm{inter}} \sum_i \boldsymbol{m}_i^{\mathrm{T}} \cdot \boldsymbol{m}_i^{\mathrm{B}}. \tag{4}$$

The symbol of A_{inter} is negative for the interlayer AFM interaction, where we assume that spins in the top FM layer are pointing upward and the spins in the bottom FM layer are pointing downward owing to the interlayer AFM exchange coupling. The strong antiferromagnetic coupling results in the two FM layers having opposite magnetization configurations, which plays a key role in eliminating the skyrmion Hall effect.[60]

Here, we simulate the SAF skyrmion logic functions using the Object Oriented Micromagnetic Framework (OOMMF) with an extended module of the Dzyaloshinskii–Moriya interaction.[61] For micromagnetic simulations, the standard magnetic material parameters of Co/Pt multilayers are used for the SAF structure:[27,29,42,45,59] $M_{\mathrm{S}} = 580\ \mathrm{kA{\cdot}m^{-1}}$, $K = 0.65\ \mathrm{MJ{\cdot}m^{-3}}$–$0.85\ \mathrm{MJ{\cdot}m^{-3}}$ with a default value of $K = 0.8\ \mathrm{MJ{\cdot}m^{-3}}$, $A_{\mathrm{intra}} = 15\ \mathrm{pJ{\cdot}m^{-1}}$, $D = 2.9\ \mathrm{mJ{\cdot}m^{-2}}$–$3.3\ \mathrm{mJ{\cdot}m^{-2}}$ with a default value of $D = 3\ \mathrm{mJ{\cdot}m^{-2}}$, antiferromagnetic coupling strength $A_{\mathrm{inter}} = 4\ \mathrm{mJ{\cdot}m^{-2}}$, $\gamma_0 = 2.211 \times 10^5\ \mathrm{m{\cdot}(A{\cdot}s)^{-1}}$, $\alpha = 0.3$. Considering the balance between the numerical accuracy and computational efficiency, all the cell size used in this simulation is 2 nm×2 nm×1 nm.

For the steady motion of skyrmion in the proposed SAF logic gates, we use the Thiele equation to interpret the simulation results of isolated skyrmion.[46,51,62,63] The current-induced skyrmion motion in a bilayer nanotrack can be written as

$$\boldsymbol{G} \times \boldsymbol{v} - \alpha \boldsymbol{D}_{\mathrm{diss}} \cdot \boldsymbol{v} + 4\pi \boldsymbol{B} \cdot j + \frac{\boldsymbol{F}_{\mathrm{edge}}}{b} = \boldsymbol{0}, \tag{5}$$

where $\boldsymbol{v}$, α, $\boldsymbol{D}_{\mathrm{diss}}$, and $\boldsymbol{B}$ represent the skyrmion velocity, the damping constant, the dissipative tensor, and the tensor related to the driving current, respectively. In the fourth term, $\boldsymbol{F}_{\mathrm{edge}}$ is the external force that includes the joint repulsive force from the tilted edge and notches, where the constant $b = \mu_0 a M_{\mathrm{s}}/\gamma_0$. $\boldsymbol{G} = (0, 0, -4\pi Q)$ is the gyromagnetic coupling vector, with Q being the skyrmion topological number.[64] The skyrmion

number in each FM layer can be defined as

$$Q = \frac{1}{4\pi}\iint \boldsymbol{m}\cdot\left(\frac{\partial \boldsymbol{m}}{\partial x}\times\frac{\partial \boldsymbol{m}}{\partial y}\right)\mathrm{d}x\mathrm{d}y. \tag{6}$$

The dissipative tensor can be written as

$$\boldsymbol{D}_{\mathrm{diss}} = 4\pi\begin{pmatrix} D_{xx} & 0 \\ 0 & D_{yy}\end{pmatrix}$$

with $D_{\mathrm{diss}} = D_{xx} = \int \partial_x \boldsymbol{m}\cdot\partial_x \boldsymbol{m}\,\mathrm{d}x\mathrm{d}y$, and the driving force term with the tensor can be written as

$$\boldsymbol{B} = \frac{\gamma_0 u}{j}\begin{pmatrix} -I_{xy} & 0 \\ 0 & I_{yx}\end{pmatrix}$$

with $I = I_{xy} = \int (\partial_x \boldsymbol{m}\times\boldsymbol{m})_y\,\mathrm{d}x\mathrm{d}y$. The last term of Eq. (5) can be written as

$$\frac{\boldsymbol{F}_{\mathrm{edge}}}{b} = \frac{1}{b}\begin{pmatrix}\boldsymbol{F}_{x-\mathrm{edge}} \\ \boldsymbol{F}_{y-\mathrm{edge}}\end{pmatrix}$$

with $\boldsymbol{F}_{x-\mathrm{edge}}$ and $\boldsymbol{F}_{y-\mathrm{edge}}$ representing edge forces in the x and y directions, respectively. For the rigid magnetic skyrmion in this work, we always have $D_{xx} = D_{yy} = D_{\mathrm{diss}}$, $I_{xy} = -I_{yx} = I$, and the value of I and D_{diss} are positive. Namely, the motion equation of isolated SAF skyrmion can be rewritten into the following form

$$\begin{pmatrix} 4\pi Q v_y \\ -4\pi Q v_x\end{pmatrix} - 4\pi\alpha\begin{pmatrix} D_{xx} & 0 \\ 0 & D_{yy}\end{pmatrix}\begin{pmatrix} v_x \\ v_y\end{pmatrix}$$

$$-4\pi\frac{\gamma_0 u}{j}\begin{pmatrix} -I_{xy} & 0 \\ 0 & I_{yx}\end{pmatrix}\begin{pmatrix} j_x \\ j_y\end{pmatrix} + \frac{1}{b}\begin{pmatrix} F_{x-\mathrm{edge}} \\ F_{y-\mathrm{edge}}\end{pmatrix} = 0, \tag{7}$$

where the spin-polarized current flows along the x direction ($j_y = 0$). Considering the steady motion of skyrmion along the nanotrack, boundary forces in the x and y directions can be ignored. Further, the topologic number of the SAF bilayer skyrmion is zero and the velocity could be simplified as

$$v_x = \frac{\gamma_0 u I}{\alpha D_{\mathrm{diss}}}, \quad v_y = 0. \tag{8}$$

According to Refs. [51,59], $I = \pi R/4$ and $D_{\mathrm{diss}} = (2R^2+\Delta^2)/\Delta R$ for a rigid skyrmion with $v_y = 0$. R is the skyrmion radius which can be calculated as $R \approx \Delta/\sqrt{2(1-D/Dc)}$, where $\Delta = \sqrt{A_{\mathrm{intra}}/K_{\mathrm{eff}}}$ is the well-known Bloch wall width parameter and $D_{\mathrm{C}} = 4\sqrt{A_{\mathrm{intra}}K/\pi}$ ($K_{\mathrm{eff}} = K - (1/2)\mu_0 M_{\mathrm{s}}^2$ can be seen as an effective anisotropy constant).[65] The theoretical solutions show that the isolated skyrmion in the SAF monolayer steadily moves along the x direction, and the velocity of the isolated SAF skyrmion is proportional to the driving force, which is consistent with the simulation results.

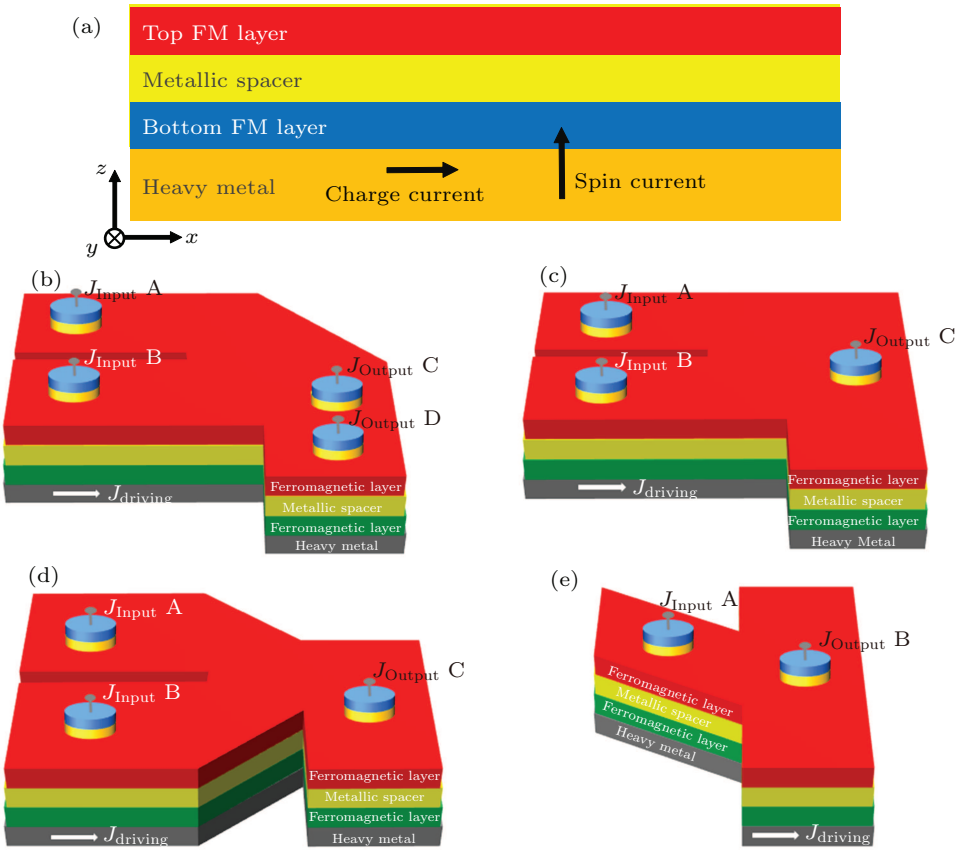
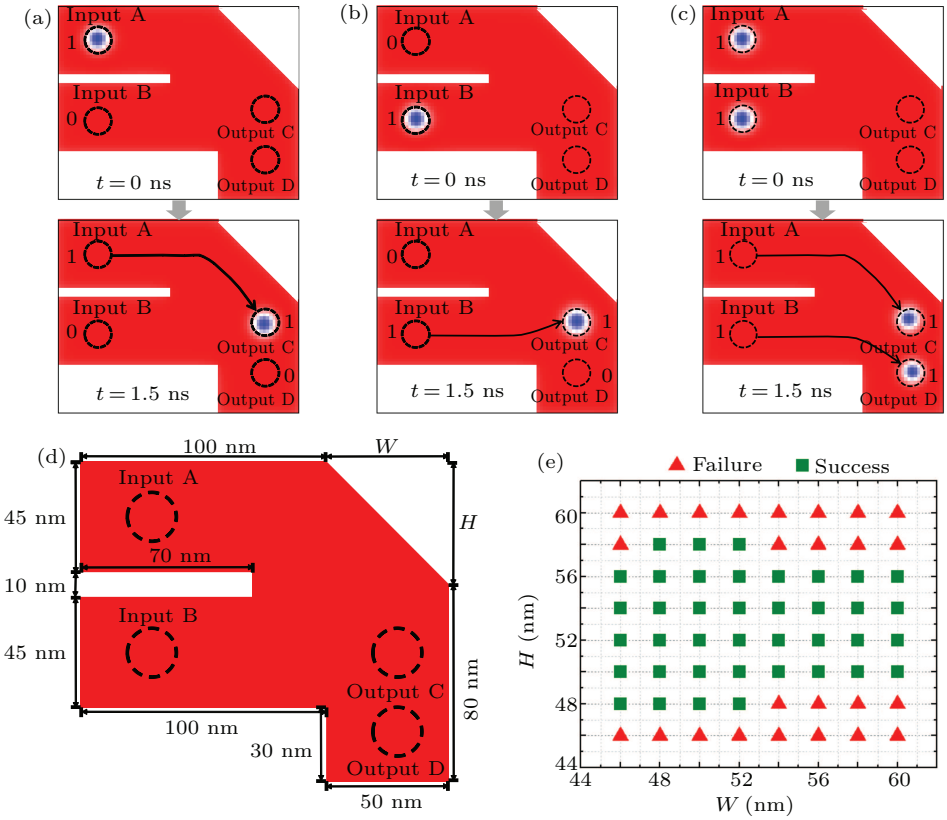


Fig. 1. Schematic diagram of the antiferromagnetically exchange-coupled bilayer system and the proposed structure of logic gates. (a) The antiferromagnetically-coupled bilayer structure for the motion of a bilayer-skyrmion driven by the spin current, where we apply electric current in the HM layer to produce a vertical spin current to the magnetic layer; (b) the illustration of skyrmion logic AND and logic OR gates with two inputs and two outputs; (c) the illustration of skyrmion logic XOR and logic NOR gates with two inputs and one output; (d) the illustration of skyrmion logic NAND gate with two inputs and one output; (e) the illustration of skyrmion logic NOT gate with one input and one output.

3. Results and discussion

3.1. Realization of OR and AND logic functions

The proposed structure of the logic OR gate is shown in Fig. 1(b), input A and input B are placed on the left side of the nanotrack and the output C is placed on the upper right side as well as a triangular notch on the right side of the nanotrack. Here, the presence of a skyrmion represents the data bit "1" and the absence of a skyrmion represents the data bit "0". When no skyrmion is created at inputs A and C, the logical operations OR "$0+0=0$" can be implemented. As shown in Fig. 2(a) and supplementary video S1, the generated isolated skyrmion at the input A moves along the $+x$ direction due to the spin torque and deviates to the $-y$ direction, and finally stops at the output C because of the notch boundary repulsion. Similarly, when a nucleated skyrmion at the input B moves along the nanotrack, it stops at the same site as the right region, as suggested by Fig. 2(b) and supplementary video S2. Thus, the logical operations OR "$1+0=1$" and "$0+1=1$" can be implemented successfully. However, when both skyrmions from input A and input B move in this nanotrack as shown in Fig. 2(c) and supplementary video S3, the bottom skyrmion created at input B can stop at the lower side of the right region once it meets with the top skyrmion. As a result, the logical operation OR "$1+1=1$" can be implemented.



(f)

Logic OR		
Input A	Input B	Output C
0	0	0
1	0	1
0	1	1
1	1	1

(g)

Logic AND		
Input A	Input B	Output C
0	0	0
1	0	0
0	1	0
1	1	1

Fig. 2. The micromagnetic simulations for the logic AND and OR gates in the SAF nanotrack. (a)–(c) The micromagnetic simulations of three cases for the logic AND and OR gates in the SAF nanotrack. (d) The top view of the logic OR and AND structure, where the black dashed circles represent the input and output MTJs. (e) The working window of the notch size in the logic AND and OR structure. (f)–(g) The truth tables for logic OR and AND gates.

The logic function of AND can be implemented in the same structure as the OR logic gate by changing the detection region as depicted in Fig. 1(b). When the lower right region is set as the output D, the logic function "$1\cdot 0=0$" and "$0\cdot 1=0$" of AND are similar to the function of the OR gate which can be implemented as depicted in Figs. 2(a)–2(b) and supplementary videos S1 and S2. In this structure, regardless of whether the isolated skyrmion is at input A or input B, it cannot reach input D under $+x$ direction driving current. Only when two skyrmions move along the $+x$ direction from input A and input B simultaneously, the bottom skyrmion nucleated at the input B can be squeezed into the output D region due to the skyrmion–skyrmion interaction as shown in Fig. 2(c) and supplementary video S3. Namely, the logical operation

AND "$1 \cdot 1 = 1$" can be implemented. It is noted that when no skyrmion exists for both inputs, there is no data transmission on the nanotrack and the logical operation AND "$0 \cdot 0 = 0$" is achieved. Here, the height (H) and the base (W) length of the triangle influence the final stable position of the bottom skyrmion as shown in the top-view of the structure (Fig. 2(d)), where the phase diagram of logical operations and the working window of the input position of AND and OR gates are provided in Fig. 2(e) and video S6(a). The corresponding truth tables for the logic OR and AND gates are shown in Figs. 2(f) and 2(g).

3.2. Realization of XOR and NOR logic functions

The SAF bilayer XOR and NOR gates can be achieved with a structure similar to the AND gate as shown in Fig. 1(c), input A and input B are at the left side of the F-type nanotrack, while output C is at the center of the right side. The difference between logic XOR and OR gates is that they lack the triangular notch in the upper right. In this regime, when no skyrmion is created in the inputs A and B, the logic operation of XOR gate "$0 \oplus 0 = 0$" can be realized. As shown in Figs. 3(a)–3(b) and supplementary videos S4 and S5, only one skyrmion is created in input A or input B. The skyrmion is driven by the spin current and then stops at the center of the right side due to the skyrmion–edge repulsion. Thus, the logic operation of XOR gate "$1 \oplus 0 = 1$" and "$0 \oplus 1 = 1$" can be implemented. However, when two skyrmions are created in inputs A and B, the two skyrmion driven by the spin current will push one another away from the center of the right nanotrack and output data bit "0" as shown in Fig. 3(c) and supplementary video S6. In addition, the working window of the input position of XOR gate is given in video S6(a). So, the logic operation of XOR gate "$1 \oplus 1 = 0$" can also be implemented.

The SAF bilayer NOR logic gate is proposed with the same structure as the XOR gate. Initially, a skyrmion is already nucleated at the output C. In this regime, as shown in Fig. 3(d) and supplementary video S7, when no skyrmion is created in the input A and B, the skyrmion in the center of the right side of the nanotrack remains stationary and the logic operation of the NOR gate "$\overline{0+0} = 1$" can be realized. However, when an individual skyrmion is created at the input A or B, driving by the $+x$ direction current, the left skyrmion will meet with the right one and push one another away from the center of the right nanotrack due to the skyrmion–skyrmion repulsion. Therefore, the logic operation of NOR "$\overline{1+0} =$" and "$\overline{0+1} =$" can be implemented as shown in Figs. 3(e)–3(f) and supplementary videos S8 and S9. Furthermore, if two skyrmions are nucleated in input A and input B, the skyrmion in output C will be annihilated by the repulsion between the skyrmions, and the two skyrmions created from the left side are going to push one another away from the center of the right region as shown in Fig. 3(g) and supplementary video S10. In addition, the working window of the input position of NOR gate is given in video S6(a). Namely, the operation of the NOR gate "$\overline{1+1} = 0$" can be realized.



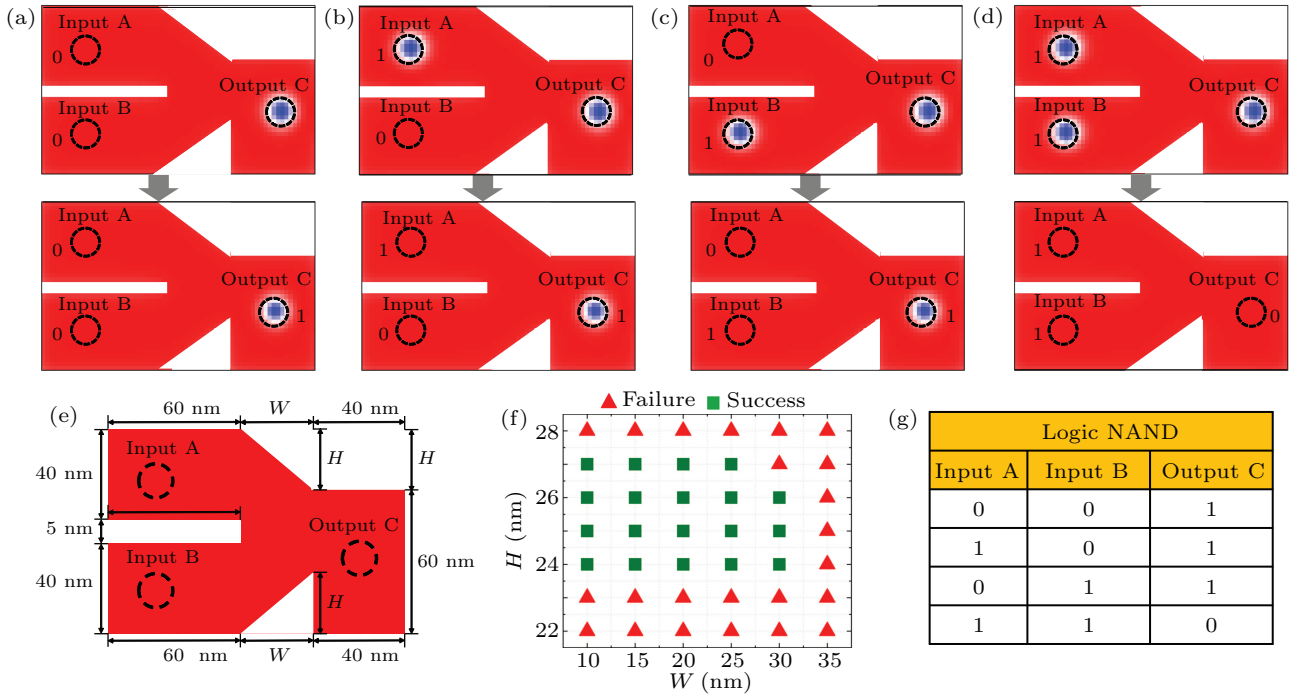
Logic XOR		
Input A	Input B	Output C
0	0	0
0	1	1
1	0	1
1	1	0

Logic NOR		
Input A	Input B	Output C
0	0	0
0	1	0
1	0	0
1	1	0

Fig. 3. The micromagnetic simulations and truth tables for the logic XOR and NOR gates in the SAF nanotrack. (a)–(c) Three cases of inputs and their corresponding micromagnetic simulations for the logic XOR gate in the nanotrack. (d)–(g) Four cases of inputs and their corresponding micromagnetic simulations for the NOR gate in the nanotrack. (h) The truth tables of the logic XOR and NOR gates.

3.3. Realization of NAND logic function

The logic function of NAND can be implemented in the proposed structure as shown in Fig. 1(d). Here shows a triangular notch is on the lower right side and a trapezoidal notch is on the upper right side. Input A and B are placed on the left side of the nanotrack, while the output C is placed at the center of the right side. Similar to the logic NOR gate, there is an individual skyrmion at the center of the right-side nanotrack initially as shown in Fig. 4(a) and supplementary video S11. When both inputs data bit are "0", there is no skyrmion moving in the SAF nanotrack and output "1" state and the logical operation of NAND "$\overline{0\cdot 0}=1$" can be implemented. As shown in Figs. 4(b)–4(c) and supplementary videos S12 and S13, considering only one skyrmion is created at the left input A or B, the left skyrmion will annihilate as it moves along the nanotrack at the boundary due to edge geometry confined. Hence, the operation of "$\overline{1\cdot 0}=1$", and "$\overline{0\cdot 1}=1$" can be carried out. The most important operation of "$\overline{1\cdot 1}=0$" is implemented by the presence of skyrmions in both input A and B. As shown in Fig. 4(d) and supplementary video S14, all skyrmions in this operation will annihilate due to the skyrmion–skyrmion repulsion and skyrmion–edge repulsion. Here, the height (H) and the base (W) length of the triangle influence the state of the left skyrmion as shown in the top-view of the structure (Fig. 4(e)). In addition, the phase diagram of the operations, the working window of the input position of NAND gate and corresponding truth tables for NAND gates are given in Figs. 4(f)–4(g) and video S6(b).



Logic NAND		
Input A	Input B	Output C
0	0	1
1	0	1
0	1	1
1	1	0

Fig. 4. The simulation results of logic NAND gate with two notches. (a)–(d) The micromagnetic simulations of four cases of inputs for the logic NAND gate in the SAF nanotrack. (e) The top view of the logic NAND structure. (f) The working window of the notch size in the logic NAND structure. (g) The truth table of the logic NAND.

3.4. Realization of NOT logic function

The logic NOT gate is implemented in a y-junction structure as shown in Fig. 1(e). There are two nanotracks, where the input terminal A is at the left nanotrack and the output terminal B is at the center of the right nanotrack. Note an isolated skyrmion is initially nucleated in the center of the right nanotrack, as shown in Fig. 5(a) and supplementary video S15. When no skyrmion is created in the left nanotrack, namely input data bit "0", the skyrmion in the center of the nanotrack remains at its original position due to the edge-skyrmion repulsion and output data bit "1". Hence, the NOT gate "$\bar{0}=1$" is accomplished. A skyrmion is created in the left nanotrack and driven by a $+x$ direction spin current. In that case, the left skyrmion will meet the right skyrmion and rotate at an angle of 90° and push one another away from the center of the right nanotrack as shown in Fig. 5(b) and supplementary video S16. And the working window of the input position of NOT gate is also given in video S6(c). Therefore, the logic function of NOT gate "$\bar{1}=0$" has also been implemented.

In particular, a logic switching delay is determined by the skyrmion velocity and the distance between the input and output terminals.[45,49] Therefore, the trade-off between skyrmion-based logic gates' response speed and energy consumption needs to be considered.[48] Namely, a smaller driving current can decrease the energy consumption and a large current can be adopted for high switching speed. As shown in

Fig. 6(a), the driving current of the above logic gates should be limited to 1×10^{11} A·m^2–4×10^{11} A·m^2, and SAF skyrmion velocity is proportional to the driving current density, where the larger current density may lead to SAF skyrmion annihilation at the right side due to large spin orbit torque. Figure 6(b) shows that the magnetic material parameters such as K and D can also affect the skyrmion velocity, where the velocity increases as D increases and decreases as K increases in the above logic gates. Moreover, the skyrmion size can effectively reduce the scale of the logic devices and influence the distance between the input and output terminal, which can be determined by magnetic material parameters such as PMA and DMI constants. Figure 6(c) shows that the diameter of the skyrmion increases as D increases and decreases as K increases. Hence, the switching delay can be affected by downscale of the logic gates via adjusting magnetic parameters.

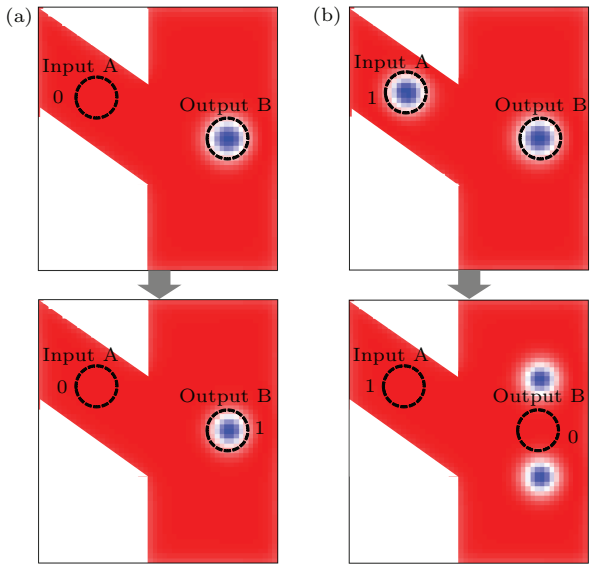


Fig. 5. The simulation results of logic NOT gate. (a) The logical operation of NOT gate $\bar{0}=1$ on SAF nanotrack. (b) The logical operation of NOT gate $\bar{1}=0$ on SAF nanotrack.

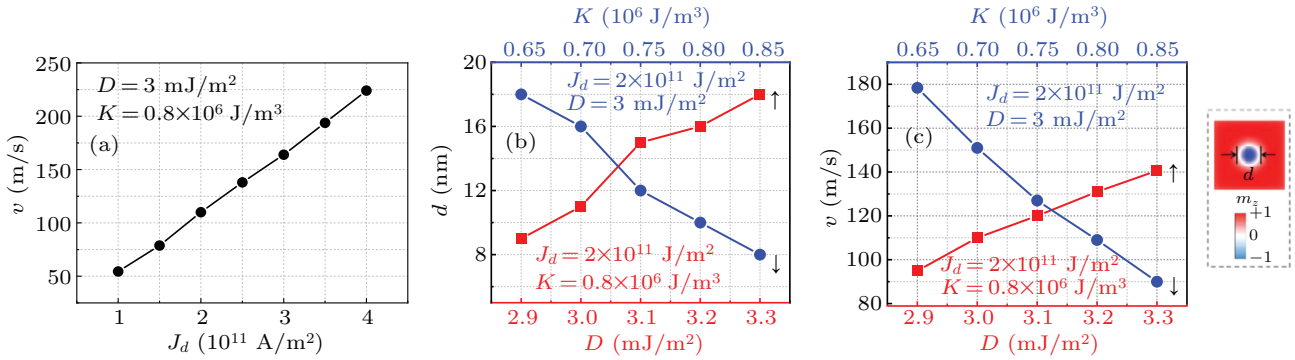


Fig. 6. Skyrmion velocity and skyrmion size vary with the current density and material parameters. (a) Simulation results of the motion velocity of isolated skyrmion vary with the current density. (b) Simulation results of the motion velocity with the PMA constant (K) and DMI constant (D). (c) The skyrmion diameter varies with PMA constant (K) and DMI constant (D).

4. Conclusion

In conclusion, we theoretically study the skyrmion velocity in the SAF monolayer, which indicates that the skyrmion velocity can be influenced by the driving force and the edge of the nanotrack. The theoretical results are consistent with the numerical simulation results. By designing geometric notches and tilted edges on the SAF nanotracks, we have proposed six basic logic gates based on the motion of SAF skyrmion, including the logic AND, OR, NOR, XOR, NOT, and NAND gates, which are implemented by spin–orbit torque, skyrmion Hall effect, skyrmion–skyrmion repulsion, and skyrmion–edge interaction. The proposed SAF skyrmion-based logic gates in this work have potential application in the future topological magnetic devices.

Data availability statement

The data that support the findings of this study are openly available in Science Data Bank at the following link http://doi.org/10.57760/sciencedb.j00113.00066.

Acknowledgements

Guoping Zhao acknowledges the support from the National Natural Science Foundation of China (Grant Nos. 51771127, 52171188, and 52111530143) and the Central Government Funds of Guiding Local Scientific and Technological Development for Sichuan Province, China (Grant No. 2021ZYD0025). Jing Xia was a JSPS International Research Fellow supported by JSPS KAKENHI (Grant No. JP22F22061). Yan Zhou acknowledges the support from Guangdong Basic and Applied Basic Research Foundation (Grant No. 2021B1515120047), Guangdong Special Support Project (Grant No. 2019BT02X030), Shenzhen Fundamental Research Fund (Grant No. JCYJ20210324120213037), Shenzhen Peacock Group Plan (No. KQTD20180413181702403), Pearl River Recruitment Program of Talents (Grant No. 2017GC010293), and the National Natural Science Foundation of China (Grant Nos. 11974298 and 61961136006). Xiaoxi Liu acknowledges the support from the Grants-in-Aid Scientific Research from JSPS KAKENHI (Grant Nos. JP20F20363, JP21H01364, and JP21K18872).

References

[1] Skyrme T H R 1962 *Nucl. Phys.* **31** 556
[2] Bogdanov A N and Yablonskii D A 1989 *J. Exp. Theor. Phys.* **68** 101
[3] Bogdanov N and Hubert A 1994 *J. Magn. Magn. Matter.* **138** 255
[4] Wright D C and Mermin N D 1989 *Rev. Mod. Phys.* **61** 385
[5] Rößler U K, Bogdanov A N and Pfleiderer C 2006 *Nature* **442** 797
[6] Tewari S, Belitz D and Kirkpatrick T R 2006 *Phys. Rev. Lett.* **96** 047207
[7] Binz B, Vishwanath A and Aji V 2006 *Phys. Rev. Lett.* **96** 207202
[8] Mühlbauer S, Binz B, Jonietz F, Pfleiderer C, Rosch A, Neubauer A, Georgii R and Boni P 2009 *Science* **323** 915
[9] Boulle O, Vogel J, Yang H X, Pizzini S, Chaves D D, Locatelli A, Mentes T O, Sala A, Buda-Prejbeanu L D, Klein O, Belmeguenai M, Roussigne Y, Stashkevich A, Cherif S M, Aballe L, Foerster M, Chshiev M, Auffret S, Miron I M and Gaudin G 2016 *Nat. Nanotechnol.* **11** 449
[10] Yu G Q, Upadhyaya P, Li X, Li W Y, Kim S K, Fan Y B, Wong K L, Tserkovnyak Y, Amiri P K and Wang K L 2016 *Nano Lett.* **16** 1981
[11] Yang H X, Thiaville A, Rohart S, Fert A and Chshiev M 2015 *Phys. Rev. Lett.* **115** 267210
[12] Yu G Q, Jenkins A, Ma X, Razavi S A, He C L, Yin G, Shao Q M, He Q L, Wu H, Li W J, Jiang W J, Han X F, Li X Q, C. J B A, Amiri P K and Wang K L 2018 *Nano Lett.* **18** 980
[13] Wang L, Liu C, Mehmood N, Han G, Wang Y D, Xu X L, Feng C, Hou Z P, Peng Y, Gao X S and Yu G H 2019 *ACS Appl. Mater. Interfaces* **11** 12098
[14] Moreau-Luchaire C, Mouta S, Reyren N, Sampaio J, Vaz C A F, Van Horne N, Bouzehouane K, Garcia K, Deranlot C, Warnicke P, Wohlhuter P, George J M, Weigand M, Raabe J, Cros V and Fert A 2016 *Nat. Nanotechnol.* **11** 444
[15] Ye C, Li L L, Shu Y, Li Q R, Xia J, Hou Z P, Zhou Y, Liu X X, Yang Y Y and Zhao G P 2022 *Rare Met.* **41** 2200
[16] Zhang J Y, Zhang Y, Gao Y, Zhao G P, Qiu L, Wang K Y, Dou P W, Peng W L, Zhuang Y, Wu Y F, Yu G Q, Zhu Z Z, Zhao Y C, Guo Y Q, Zhu T, Cai J W, Shen B G and Wang S G 2020 *Adv. Mater.* **32** 1907452
[17] Tang J, Kong L Y, Wang W W, Du H F and Tian M l 2019 *Chin. Phys. B* **28** 087503
[18] Kang W, Huang Y Q, Zhang X C, Zhou Y and Zhao W S 2016 *Proc. IEEE* **104** 2040
[19] Finocchio G, Büttner F, Tomasello R, Carpentieri M and Kläui M 2016 *J. Phys. D: Appl. Phys.* **49** 423001
[20] Yu G Q, Upadhyaya P, Shao Q M, Wu H, Yin G, Li X, He C L, Jiang W J, Han X F, Amiri P K and Wang K L 2017 *Nano Lett.* **17** 261
[21] Fert A and Van Dau F N 2019 *C. R. Phys.* **20** 817
[22] Zhao W S, Huang Y Q, Zhang X Y, Kang W, Lei N and Zhang Y G 2018 *Acta Phys. Sin.* **67** 131205 (in Chinese)
[23] Xing X J, Pong P W T and Zhou Y 2016 *Phys. Rev. B* **94** 054408
[24] Zhou Y and Ezawa M 2014 *Nat. Commun.* **5** 4652
[25] Liang X, Zhao L, Qiu L, Li S, Ding L H, Feng Y H, Zhang X C, Zhou Y and Zhao G P 2018 *Acta Phys. Sin.* **67** 137510 (in Chinese)
[26] He Z Z, Angizi S and Fan D L 2017 *IEEE Magn. Lett.* **8** 4305705
[27] Luo S J, Song M, Li X, Zhang Y, Hong J, Yang X F, Zou X C, Xu N and You L 2018 *Nano Lett.* **18** 1180
[28] Chauwin M, Hu X, Garcia-Sanchez F, Betrabet N, Paler A, Moutafis C and Friedman J S 2019 *Phys. Rev. Appl.* **12** 064053
[29] Sampaio J, Cros V, Rohart S, Thiaville A and Fert A 2013 *Nat. Nanotechnol.* **8** 839
[30] Duine R A, Lee K J, Parkin S S P and Stiles M D 2018 *Nat. Phys.* **14** 217
[31] Fattouhi M, Mak K Y, Zhou Y, Zhang X, Liu X X and El Hafidi M 2021 *Phys. Rev. Appl.* **16** 014040
[32] Xia J, Han Z Y, Song Y F, Jiang W J, Lin L R, Zhang X C, Liu X X and Zhou Y 2018 *Acta Phys. Sin.* **67** 137505 (in Chinese)
[33] White J S, Prsa K, Huang P, Omrani A A, Zivkovic I, Bartkowiak M, Berger H, Magrez A, Gavilano J L, Nagy G, Zang J and Ronnow H M 2014 *Phys. Rev. Lett.* **113** 107203
[34] Liu Y Z, Yin G, Zang J D, Shi J and Lake R K 2015 *Appl. Phys. Lett.* **107** 152411
[35] Zhang X C, Ezawa M, Xiao D, Zhao G P, Liu Y W and Zhou Y 2015 *Nanotechnology* **26** 225701
[36] Okamura Y, Kagawa F, Seki S and Tokura Y 2016 *Nat. Commun.* **7** 12669
[37] Yu X Z, Kanazawa N, Zhang W Z, Nagai T, Hara T, Kimoto K, Matsui Y, Onose Y and Tokura Y 2012 *Nat. Commun.* **3** 988
[38] Lin S Z, Batista C D, Reichhardt C and Saxena A 2014 *Phys. Rev. Lett.* **112** 187203
[39] Zhang W, Jungfleisch M B, Freimuth F, Jiang W, Sklenar J, Pearson J E, Ketterson J B, Mokrousov Y and Hoffmann A 2015 *Phys. Rev. B* **92** 144405
[40] Zhang X C, Zhao G P, Fangohr H, Liu J P, Xia W X, Xia J and Morvan F J 2015 *Sci. Rep* **5** 7643
[41] Fert A, Cros V and Sampaio J 2013 *Nat. Nanotechnol.* **8** 152
[42] Zhang X C, Zhou Y and Ezawa M 2016 *Nat. Commun.* **7** 10293
[43] Dohi T, DuttaGupta S, Fukami S and Ohno H 2019 *Nat. Commun.* **10** 5153
[44] Legrand W, Maccariello D, Ajejas F, Collin S, Vecchiola A, Bouzehouane K, Reyren N, Cros V and Fert A 2020 *Nat. Mater.* **19** 34
[45] Mak K Y, Xia J, Zhang X C, Li L, Fattouhi M, Ezawa M, Liu X X and Zhou Y 2022 *Rare Met.* **41** 2249
[46] Thiele A A 1973 *Phys. Rev. Lett.* **30** 230
[47] Ma X P, Piao H G, Yang L, Kim D H, You C Y and Pan L Q 2020 *Chin Phys. B* **29** 097502
[48] Zhang X C, Ezawa M and Zhou Y 2015 *Sci. Rep* **5** 9400
[49] Luo S J and You L 2021 *APL Mater.* **9** 050901
[50] Lin S Z, Reichhardt C, Batista C D and Saxena A 2013 *Phys. Rev. B* **87** 214419
[51] Shen L C, Xia J, Zhao G P, Zhang X C, Ezawa M, Tretiakov O A, Liu X X and Zhou Y 2019 *Appl. Phys. Lett.* **114** 042402
[52] Weisheit M, Fahler S, Marty A, Souche Y, Poinsignon C and Givord D 2007 *Science* **315** 349
[53] Maruyama T, Shiota Y, Nozaki T, Ohta K, Toda N, Mizuguchi M, Tulapurkar A A, Shinjo T, Shiraishi M, Mizukami S, Ando Y and Suzuki Y 2009 *Nat. Nanotechnol.* **4** 158
[54] Woo S, Mann M, Tan A J, Caretta L and Beach G S D 2014 *Appl. Phys. Lett.* **105** 212404
[55] Cheng R, Xiao J, Niu Q and Brataas A 2014 *Phys. Rev. Lett.* **113** 057601
[56] Jiang W J, Zhang X C, Yu G Q, Zhang W, Wang X, Jungfleisch M B, Pearson J E, Cheng X M, Heinonen O, Wang K L, Zhou Y, Hoffmann A and te Velthuis S G E 2016 *Nat. Phys.* **13** 162
[57] Kong L and Zang J 2013 *Phys. Rev. Lett.* **111** 067203
[58] Zhao L, Liang X, Xia J, Zhao G P and Zhou Y 2020 *Nanoscale* **12** 9507
[59] Xia J, Zhang X C, Mak K Y, Ezawa M, Tretiakov O A, Zhou Y, Zhao G P and Liu X X 2021 *Phys. Rev. B* **103** 174408
[60] Liang X, Zhao G P, Shen L C, Xia J, Zhao L, Zhang X C and Zhou Y 2019 *Phys. Rev. B* **100** 144439
[61] Donahue M J and Porter DG 1999 *Interagency Report NISTIR* 6376
[62] Iwasaki J, Mochizuki M and Nagaosa N 2013 *Nat. Commun.* **4** 1463
[63] Iwasaki J, Koshibae W and Nagaosa N 2014 *Nano Lett.* **14** 4432
[64] Nagaosa N and Tokura Y 2013 *Nat. Nanotechnol.* **8** 899
[65] Rohart S and Thiaville A 2013 *Phys. Rev. B* **88** 184422